



# Study of ultrasonic additive manufacturing and its utilization for the production of aluminum components made of alloys of the AA5XXX series

Jean-Nicolas Rousseau<sup>1,2</sup> · Alexandre Bois-Brochu<sup>1,2</sup> · Nicolas Giguère<sup>1,2</sup> · Carl Blais<sup>2</sup>

Received: 8 September 2021 / Accepted: 7 December 2021 / Published online: 28 January 2022  
© The Author(s), under exclusive licence to Springer-Verlag London Ltd., part of Springer Nature 2022

## Abstract

Ultrasonic welding additive manufacturing (UWAM) enables the production of metallic components by forming metallurgical bonds between superimposed thin foils using continuous ultrasonic welding. The aluminum alloys that were considered in this study were AA5005 (0.8%-wt. Mg), AA5052 (2.4%-wt. Mg), and AA5056 (4.9%-wt. Mg). The influence of Mg content on UAM was investigated with respect to the following criteria: microstructural changes in welded foils, ultrasonic welding energy, geometry of the joints, and tensile properties along different building directions. Joint resistance was found to be correlated to the ultrasonic welding energy input, where the dominant parameters are temperature, welding speed, and the amplitude of vibration. Energy can be raised by decreasing the welding speed or by increasing the amplitude of vibration leading to better joint properties but reducing tensile properties in the two other orthotropic directions of the build. The aluminum components built by AM were characterized with having anisotropic tensile properties due to the process itself and the strain hardening of the foils during fabrication. When comparing tensile results with those of the base material, optimum tensile properties in the longitudinal direction (X) are 5% higher, identical in the transverse direction (Y), and 55% lower for specimens sampled along the direction of deposition (Z). Depending on the orientation of the tensile specimens with regard to the deposition direction (Z), strain at rupture was 25% in the X-direction and 7% along the Y-direction. No specimens could be adequately built using AA5056-H38 foils. Characterization of the few joints that could be produced showed that this behavior was due to the presence of a significant amount of Mg oxide at the interface of neighboring foils paired with a drastic increase of hardness compared to what was measured for the other alloys.

**Keywords** Ultrasonic welding additive manufacturing · AA5XXX · Tensile properties · Magnesium concentration · Process optimization

## 1 Introduction

Ultrasonic welding additive manufacturing (UWAM) combines within the same enclosure ultrasonic welding of metals and machining [1]. Thin strips are deposited by continuous ultrasonic welding, successively forming layers that may additionally be machined during manufacturing. It is therefore an intimate combination of additive and subtractive manufacturing. Ultrasonic welding is a high strain, solid-state welding process having similarities with friction accumulative roll

bonding and ultrasonic spot welding. The joints created are produced at temperatures below those of the melting point of the deposited material. The term ultrasound refers to the frequencies used (20 kHz) for the lateral movement of the sonotrode (ref. Fig. 1). The sonotrode has a surface texture that prevents the metallic strip to be deposited from sliding on its surface. The lateral oscillating movement of the sonotrode thus induces an identical lateral movement to the metallic strip without there being any slippage or loss of energy between the two. Additionally, the normal force exerted by the sonotrode, a force that is perpendicular to its axis of oscillation, imposes intense friction between the metal strip and the surface of the metal substrate on which it is deposited, thus creating oxide destabilization, localized plastic deformation, and cold welding. This technology is particularly interesting for its ability to join similar as well as dissimilar metals at low temperature. Thus, it is possible to weld reactive materials with each other

✉ Carl Blais  
carl.blais@gmn.ulaval.ca

<sup>1</sup> Quebec Metallurgy Center, Trois-Rivières, QC, Canada

<sup>2</sup> Department of Mining, Metallurgical and Materials Engineering, Université Laval, Quebec City, QC, Canada

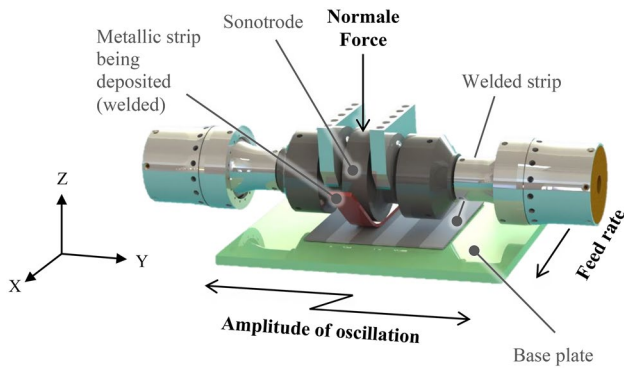


**Fig. 1** General layout of ultrasonic welding additive manufacturing (UWAM) device adapted from [2]. Text in bold refers to the deposition parameters that were studied

such as aluminum and titanium, while avoiding the formation of unwanted intermetallics.

The aluminum grades most commonly studied for the UWAM process are alloy AA3003 [3–10] as well AA6061 [1, 10–16]. On the other hand, it appears that no published manuscript discusses additive manufacturing by ultrasonic welding of Al–Mg alloys, i.e., AA5000 series. However, these have some of the best mechanical properties among non-heat-treatable Al alloys. Compared to other series typically modified by strain hardening, the addition of magnesium rapidly increases the tensile properties of the alloy [17].

Within the framework of this study, three alloys were selected: AA5005, AA5052, and AA5056. These grades have typical Mg concentrations of 1, 2.5, and 5%-wt. Alloy 3003 in the H18 state was also incorporated in this study for comparison, as it is one of the most widely used aluminum alloys in UWAM. The main objective of the present study was to characterize the benefits of the work hardening potential of AA5XXX Al alloys to fabricate AM components with high mechanical properties in the as-built condition.

## 2 Methodology

### 2.1 Materials

The standardized chemical compositions of the different strips used in this study are presented in Table 1. The exact

**Table 1** Standard chemical composition of the alloys used in this study [17]

Alloy	Elements (%-wt.)									
	Si	Fe	Cu	Mn	Mg	Cr	Zn	Other each	Other total	Bal
AA3003	0.6	0.7	0.05–0.20	1.0–1.5	-	-	0.10	0.05	0.15	Al
AA5005	0.30	0.7	0.20	0.20	0.50–1.1	0.10	0.25	0.05	0.15	Al
AA5052	0.25	0.40	0.10	0.10	2.2–2.8	0.15–0.35	0.10	0.05	0.15	Al
AA5056	0.30	0.40	0.10	0.05–0.20	4.5–5.6	0.20	0.10	0.05	0.15	Al

**Table 2** Actual chemical composition of the alloys studied

Alloy	Element (wt-%)							Bal
	Si	Fe	Cu	Mn	Mg	Cr	Zn	
AA3003	0.58	0.67	0.12	1.21	-	-	0.1	Al
AA5005	0.12	0.24	0.01	0.04	0.8	0.00	0.00	Al
AA5052	0.09	0.25	0.01	0.03	2.4	0.21	0.02	Al
AA5056	0.12	0.25	0.04	0.10	4.9	0.09	0.01	Al

compositions of the strips from the supplier are shown in Table 2. In the following tables, alloy AA3003 is included for comparison. The dimensions as well as the metallurgical states of the strips used are shown in Table 3 [17].

The mechanical properties of several rolled aluminum alloys are governed by ASTM standard B209 [18]. The prerequisites for the conventional yield strength, tensile strength, and elongation for a strip with a thickness of 150  $\mu\text{m}$  are given in Table 4. Alloy AA5056, on the other hand, is not regulated by this standard. Tensile tests were performed on the Al strips and are also reported in Table 4.

The strips used in this study were cold rolled to obtain final dimensions and mechanical properties. In an attempt to confirm certain hypotheses regarding the weldability by ultrasonic welding of alloy AA5056, a strip roll in the initial state H38 was partially annealed. Annealing was carried out under vacuum in a Vac Aero furnace model VAH2636 HV-2 to prevent the formation of MgO on the surface [19]. The strip roll was inserted into the vacuum furnace and gradually heated to a soaking temperature of 345  $^{\circ}\text{C}$ . The coil was held at that temperature for 75 min followed by natural cooling in the furnace. This latter condition is denoted AA5056-O in the remainder of the text.

### 2.2 Sample manufacturing

The samples were produced on an ultrasonic welding additive manufacturing device from Fabrisonic, model SonicLayer 4000, equipped with a 20-kHz ultrasonic generator from Dukane with a power of 4.8 kW. All samples were built on 12.7-mm-thick AA6061-T651 aluminum plates serving as a substrate.

#### 2.2.1 Ultrasound-assisted welding operations

Two series of samples were produced by UWAM. The first type is identified as “single band” meaning that the builds

**Table 3** Dimensions of the aluminum strips used in this study

Alloy	State	Thickness (μm)	Width (mm)
AA3003	H18	150	23.8
AA5005	H38	150	25.4
AA5052	H38	150	25.4
AA5056	H38	150	25.4

were made from welding single strips one on top of the other with no lateral juxtaposition. Therefore, no joints exist in the XY plane (ref. Fig. 2a). Conversely, the second series of specimens was produced by overlapping strips in the XY plane. The latter will be referred to as “blocks” (Fig. 2b) in the rest of this document. Both series of samples are made of several welded strips to achieve the necessary deposit heights for sampling tensile test specimens.

The single bands have the width of a strip (i.e., 23.8 mm for AA3003-H18 and 25.4 mm for the other alloys; ref. Table 3) and a length of 254 mm. As for the blocks, they have overall dimensions of just over 254 mm (i.e., width of 10 strips) and a length of 254 mm.

The frame of reference used for the entire study is presented in Fig. 2 and makes it possible to express both the directions associated with the rolling of the strips and their relative position within the welded parts. The references between the strip and the part are as follows:

- X-axis: Longitudinal direction of rolling (L) as well as direction of advance during welding
- Y-axis: Long transverse direction of rolling (TL) as well as direction of overlapping of the strips
- Z-axis: Normal or short transverse direction of rolling (TC) as well as direction of build

As mentioned previously, the strip deposition always took place along the X-axis, the same direction as that of the strip rolling. During the fabrication of blocks, a 142-μm thickness increment was used along the Z-axis. This increment was found to be optimum for welding 150-μm aluminum strips considering the reduction in strip thickness as a result of welding. Prior to welding each new layer of a block, a translation along the Y-axis was performed to

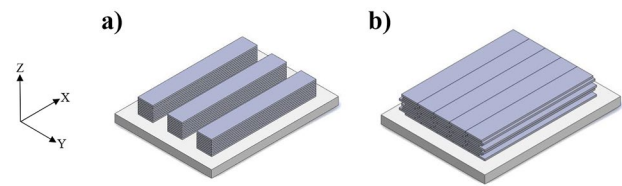


**Fig. 2** Two series of UWAM specimens were produced in this study: (a) single bands, i.e., stacked single strips, and (b) blocks

avoid the vertical alignment of the joints (ref. Fig. 3). This operation is only performed during block production, since no vertical seams are present when welding single strips. These steps are then repeated until the desired structural height is reached.

The translation pattern used for each welded layer is presented in Fig. 4 where the “0” position represents the initial position. In other words, layers # 1 and # 3 did not experience any offset along the Y-axis. The first layer is welded directly onto the baseplate, and the pattern is repeated every 32 layer. Since the first as well as the last welded strips within a layer are not fully supported (cantilever) due to the lateral offset from layer to layer, a 20% lower normal force was used to weld these specific strips. Nevertheless, the contours of each block were all machined (side milling) to remove these irregular surfaces.

For the production of welded specimens at room temperature, the baseplate was directly bolted onto the table of the CNC machining center. For builds requiring higher temperatures, the substrate was attached to an assembly allowing the insertion of heating elements.

### 2.3 Surfacing

Before any welding operation, the baseplate was face milled to obtain a precisely levelled surface with reference to the table of the machining center as well as the sonotrode. For cases where the plate was preheated, this machining operation was carried out once the necessary temperature was reached in order to avoid any distortion caused by thermal expansion. All the surfacing steps, including those performed during welding in order to rectify the welded surface, were carried out with a 6-tooth,

**Table 4** Minimum tensile properties required of aluminum strips based on ASTM standard B209 [18] along with measured values

Alloy	Yield strength (0.2%)		Tensile strength		Elongation (50 mm)	
	Measured	ASTM B209	Measured	ASTM B209	Measured	ASTM B209
	MPa	MPa	MPa	MPa	%	%
AA3003-H18	170	165	192	186	2	1
AA5005-H38	174	-	190	179	4	1
AA5052-H38	230	221	269	269	5	2
AA5056-H38	299	-	374	-	11	-

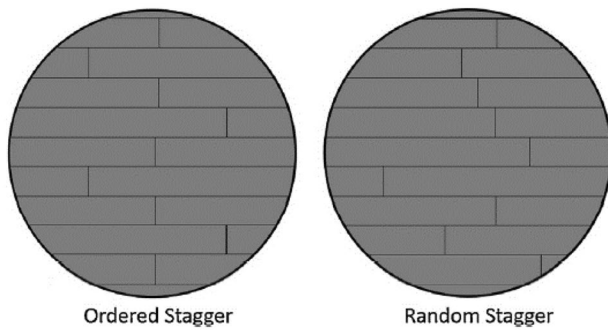


**Fig. 3** Strip layout diagram according to the YZ plane [15]

89-mm-diameter face mill at a feed rate of 21 mm/s and a rotation speed of 4 500 RPM. The milling operation was always carried out along the longitudinal direction X. Tool displacement along the Y-axis was carried out once the tool was no longer in contact with the deposited strips or the baseplate (Fig. 5). In this way, the marks left by the cutting tool were always aligned in the deposition direction, preventing potential lateral deflection of the strips during welding. In addition, no cutting fluids were used during machining operations to minimize the number of potential sources of contamination. For the same reasons, machined surfaces were systematically cleaned with isopropanol before any additive operation was initiated.

## 2.4 Deposition parameters

Although several parameters have the potential to be influential during UWAM, four of them were selected in this study. These are the normal force, the feed rate, the amplitude of oscillation, and the preheat temperature of the substrate. The selection of the minimum and maximum levels of these welding parameters was guided by preliminary tests. The levels used for the design of experiments are presented in Table 5. It is to note that deposition tests were performed at two temperatures, i.e., 20 °C and at 150 °C, to determine its effect on tensile properties of the welded specimens. UWAM outside these

**Fig. 4** Layer shift patterns along the long transverse direction (Y) for producing block specimens

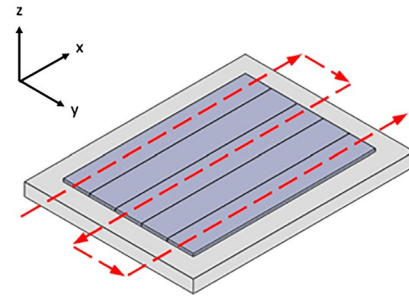
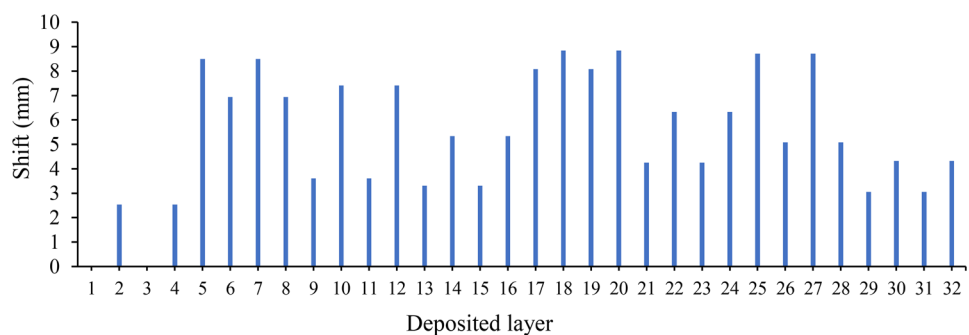


**Fig. 5** Path followed by the cutting tool during the surfacing operation

levels presented in Table 5 is possible but causes certain problems such as a decrease in the maximum height that can be welded. In order to obtain a weld quality visually equivalent to alloy AA5005-H38, the oscillation amplitude for alloy AA5052-H38 had to be 5% higher. The amplitude values reported in percentages in Table 5 correspond to the fraction of the amplitude used compared to the maximum amplitude that can be supplied by the ultrasound-assisted welding unit.

## 2.5 Tensile test samples in longitudinal and long transverse directions

Tensile specimens with a total length of 100 mm, conforming to ASTM E8/E8M [20], were used to characterize tensile properties along the longitudinal and long transverse directions. The tests were carried out on a Tinius Olsen Super L machine (398). The elongations measured are those after rupture and were measured manually by recombining the two halves of each specimen, always according to the same standard. Figure 6a shows the locations where longitudinal tensile test specimens from a “single band” were sampled. Figure 6b illustrates the locations of long longitudinal and transverse test pieces sampled from a “block.” The specimens were machined directly into the deposited strips, ensuring that no residual material from the baseplate was present. All tensile specimens had a nominal thickness of 6.35 mm.

**Table 5** Levels for the design of experiments used in this study

Factors		−1	0	+1
Normal force ( $F$ ) (N)	$x_1$	4000	5000	6000
Feed rate ( $f$ ) (mm/s)	$x_2$	64 (150 in/min)	85 (200 in/min)	106 (250 in/min)
Amplitude ( $a$ ) ( $\mu\text{m}$ )	$x_3$	30.6/32.8*	32.8/35.0*	35.0/37.2*
Amplitude (%)		65/70*	70/75*	75/80*

\*for alloy AA5052-H38

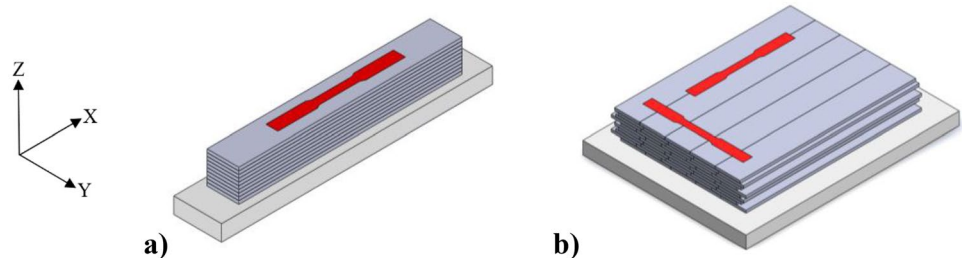
## 2.6 Short transverse direction tensile test samples

Characterization of tensile properties along the Z-axis, which corresponds to the direction of the strip deposition, is problematic. Indeed, the maximum achievable height was a limiting aspect for all the cases of our study. Thus, miniature tensile test specimens were sampled based on the work of Sridharan et al. [16]. The dimensions were the same as those reported in Fig. 7. The specimens have a parallel reduced Sect. 5 -mm long by 1.2-mm wide. Samples were taken from the center of single band specimens. First machined to match the dimensions of the outer profile, the samples were subsequently sliced by electrical discharge machining (EDM) to a nominal thickness of 0.95 mm. The tensile tests were carried out on an Instron 5565 apparatus at a constant displacement speed of 2 mm/min. Since it is not possible to use an extensometer due to the size of the samples, only the force was recorded. Figure 8 shows the location where samples were collected. The baseplate is intentionally part of one of the grip sections of the specimen.

## 2.7 Data acquisition to measure energy during deposition

A LabJack U3-HV data logger was used to record instantaneous power consumption during deposition. Power was recorded as a function of acquisition time for each welded strip and then integrated with the help of the Matlab software to obtain the energy consumed. This energy is then expressed in Joules per unit of welded area ( $\text{J}/\text{cm}^2$ ), making it possible to compare the welding energies for strips of different widths. The time interval between two measurements was fixed at 50 ms.

**Fig. 6** Sampling of tensile specimens: (a) longitudinal from a single band and (b) longitudinal and transverse long from a block



## 3 Results

### 3.1 Initial state

Figure 9 presents cross sections of the Al–Mg strips prepared along the XZ plane. The three alloys studied have, in addition to magnesium in solid solution, an appreciable amount of second-phase particles that typically have the following chemical composition [21]:  $(\text{Fe, Mn, Cr})_3\text{SiAl}_{12}$ ,  $\text{Mg}_2\text{Si}$ ,  $\text{Mg}_2\text{Al}_3$ ,  $\text{Cr}_2\text{Mg}_3\text{Al}_{18}$ . Increasing the Mg content decreases the number of particles but increases their average size as seen in the micrographs below and confirmed by image analysis. Alloy AA5056 has about twice fewer particles than alloy AA5052 and four times fewer particles than alloy AA5005. Following the same alloy order, the second-phase particles had an average external diameter of 1.44, 1.11, and 0.99  $\mu\text{m}$ , respectively. Similarly, the strips had Vickers hardness values ( $\text{HV}_{0.010}$ ) of  $105 \pm 2$ ,  $85 \pm 2$ , and  $62 \pm 1$  for grades AA5056-H38, AA5052-H38, and AA5056-H38. Following annealing, the Vickers hardness of the strips of alloy AA5056 decreased to a  $73 \pm 2$ .

The specimens built in this study were fabricated with strips in the “as-received” condition without any prior cleaning. The surface of the strips showed a very smooth surface following the final cold rolling operation. Although visually clean, the surfaces in some cases show the presence of oxides and second-phase particles. The EDS X-ray maps acquired on the surface of a AA5056-H38 strip (Fig. 10) show the presence of magnesium oxide as well as  $\text{Mg}_2\text{Si}$ .

According to these observations, the high magnesium alloy strips are the only one that displayed localized concentrations for this type of oxide on its surface. The two other alloys (AA5005 and AA5052) also showed traces of aluminum oxides, without however revealing areas rich in magnesium oxide.

### 3.2 Deposition constraints

Initial tests were carried out to characterize the surface finish of as-deposited strips (Fig. 11). The deposition parameters used to perform this work were those that correspond to the intermediate parameters in Table 5, i.e., normal force ( $F$ ) = 5000 N, feed rate ( $f$ ) = 85 mm/s, and amplitude ( $a$ ) = 35  $\mu$ m.

The significant strain hardening that takes place at the interface of welded strips affects their hardness. The graphs of Fig. 12 show hardness profiles based on Vickers micro-indentation measurements from interface to interface, i.e., across the thickness of deposited strips, for the different alloys studied. The 0- $\mu$ m position represents the lower interface ( $Z^-$ ) and the 140- $\mu$ m position represents the upper interface ( $Z^+$ ). The results are taken along the XZ plane from the central portion of single band specimens, all welded under standard parameters ( $F$  = 5000 N,  $f$  = 85 mm/s,  $a$  = 35  $\mu$ m). Figure 12a shows the hardness profiles for Al–Mg alloys in the initial state H38 and Fig. 12b for the AA5056 alloy in the H38 and O conditions. The average initial hardness of the strips is represented in the graphs by a dashed horizontal line.

Regardless of the temperature used to fabricate the specimens, the hardness at the interfaces is always greater than that observed at the center of the strips. The hardness profiles also follow the same trends whether the builds were fabricated at 20 °C or 150 °C with the difference that the values are lower at the highest temperature. When welded at room temperature, alloy AA5052-H38 displays hardness values very close to the initial strip, with higher average values at the interfaces between neighboring strips. In the case of alloy AA5005, the hardness values of the welded strips match those of the as-received material only near the interfaces between two neighboring strips. Indeed, a significant decrease in hardness is visible near the center of the strip. In the case of the strip with the highest magnesium content

(alloy AA5056), even if the partially annealed strip has a much lower initial hardness, the work hardening induced by ultrasound-assisted welding is considerable and sometimes induces increases in hardness values similar to those obtained while using H38 strips. In strongly deformed areas, always welded using the same parameters at ambient temperature, maximum hardness values of 153, 143, 92, and 85 HV<sub>0.010</sub> were measured for the strips of AA5056-H38, AA5056-O, AA5052-H38, and AA5005-H38, respectively.

The specimens produced with alloy AA5005-H38 show a significant reduction in hardness at the center of the strip compared to its initial hardness. This phenomenon is of lesser magnitude in the case of alloy AA5052-H38 and completely the opposite for grade AA5056-H38. This loss of hardness also increases with increasing build temperature (preheating). Since the fabrication of the specimens required for this study generally takes several hours, they are therefore kept at high temperatures for a considerable amount of time. Literature reports that for alloy AA5052 in the H18, exposure to similar temperatures for an extended period of time resulted in a slight decrease in mechanical properties due to recovery [19]. Since alloy AA5005-H38 contains less Mg than alloy AA5052-H38, static and dynamic recovery are favored in the case of the former alloy since dislocation glide and climb are less impeded by the solute Mg atoms [22]. As for the AA5056-H38, no effect of recovery is visible from the results acquired.

### 3.3 Maximum build height as a function of alloy chemistry

Undoubtedly, the most limiting aspect of the production of parts by UWAM is the quality of the welds between strips stacked in the short transverse direction ( $Z$ -axis). A poorly adherent interface causes delamination of the strips in subsequent welding steps, preventing the deposition of additional material. Thus, the limiting factor influencing the weldability of the different aluminum alloys used is the maximum height that can be reached by UWAM. Typical build thicknesses are presented in Table 6 according to the different alloys studied and series of samples produced. The deposition parameters used to fabricate these specimens were those that correspond to the intermediate parameters in Table 5, i.e.,  $F$  = 5000 N,  $f$  = 85 mm/s, and  $a$  = 35 mm.

Results show that it is possible to produce a UWAM deposit up to 19-mm thick using the AA3003-H18 alloy. This deposit height is also achievable with alloy AA5005-H38 but not without difficulty. For alloys with a higher magnesium content, alloy AA5052-H38 does not reach a height much higher than 7 mm, while alloy AA5056-H38/O cannot be welded. Indeed, it is possible to deposit 1.5 mm, but the quality of the joints is poor and in no way comparable to those obtained with the other alloys

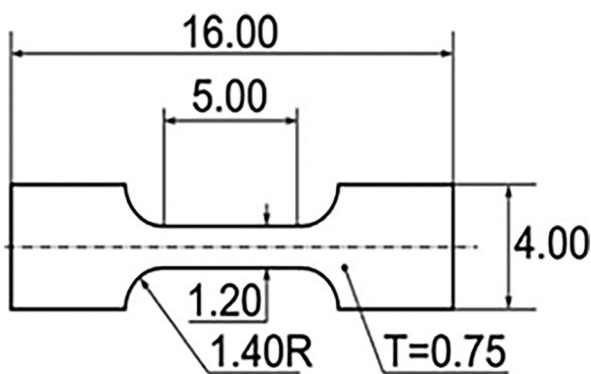


**Fig. 7** Drawing of the miniature tensile specimens proposed by Sridharan et al. [16] to characterize tensile properties along the short transverse direction (dimensions in mm)

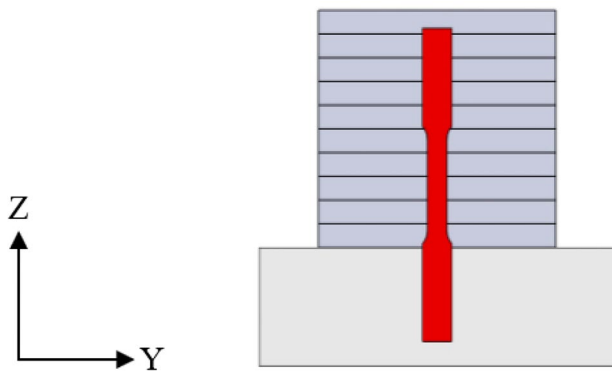


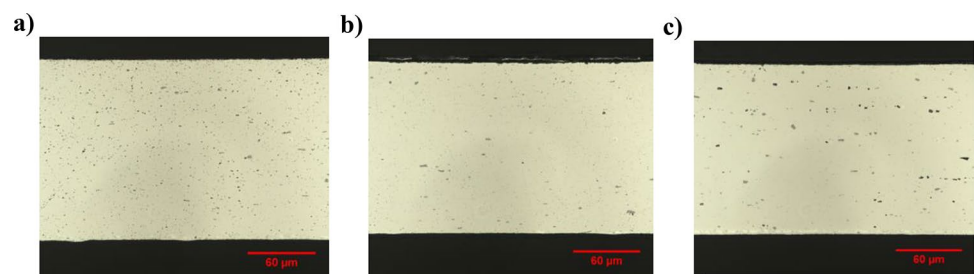
**Fig. 8** Front view of the sampling location for miniature tensile test specimens along the short transverse direction

studied. An example of such bad joints is presented in Fig. 13. Using a preheating step did not change the maximum attainable thickness. In addition, the alloys that cannot be welded to form single-strip specimens were not more weldable to produce block specimens. These results highlight the strong influence of chemistry, and therefore mechanical properties, on UWAM.

Based on these last results, tests were carried out to characterize energy transfer during deposition. Figures 14 and 15 present the variation of the deposition (welding) energy as a function of build thickness for single band specimens and block specimens, respectively. Figure 14 shows that for constant deposition parameters ( $F = 5000$  N,  $f = 85$  mm/s,  $a = 35$  m), the energy transferred to the material while building single band specimens decreases with increasing thickness. Additionally, it can be seen that the energy transferred during deposition decreases with increasing Mg concentration in the alloys. More precisely, with reference to Fig. 11b, it is seen that the decrease in energy is inversely proportional to the tensile strength of the deposited material.

In the case of block specimens, on the other hand, the results presented in Fig. 15 show that there is a marginal decrease in energy transferred as a function of increasing specimen thickness. Nonetheless, the energy decreases with increasing Mg content, i.e., increasing tensile strength.

**Fig. 9** Micrographs of the initial Al–Mg strips without etching, L–TC plane. (a) Alloy AA5005-H38, (b) alloy AA5052-H38, (c) alloy AA5056-H38



### 3.4 Effect of deposition parameters on welding energy

The energy recorded by the welding unit is a direct function of the parameters used. While a portion of this energy may potentially be absorbed in the deposition unit due to elastic deformation of certain components like the sonotrode, it is safe to assume that the vast majority of the energy supplied is channelled to the build under the form of deformation energy and heat. Thus, the energy expended by the welding unit is proportional to the energy transmitted to the part. Based on the fact that the strip is firmly gripped by the sonotrode, this energy is then in turn proportional to that distributed to the welded interface.

In order to determine what are the effects of the parameters on the welding energy, a Box-Behnken–type design of experiments was established. This plan was selected for the following reasons:

- Allows the assessment of 3 factors
- Allows the evaluation of 10 parameters, including parameter conjugations and quadratic parameters to produce the regression of Eq. 1:

$$\eta = \beta_0 + \beta_1 x_1 + \beta_2 x_2 + \beta_3 x_3 + \beta_{12} x_{12} + \beta_{13} x_{13} + \beta_{23} x_{23} + \beta_{11} x_1^2 + \beta_{22} x_2^2 + \beta_{33} x_3^2 \quad (1)$$

- Has 3 levels rather than 5 compared to centered composite planes, a particularly important factor in the present situation since the operating range for the admissible amplitudes is not very wide
- Requires fewer tests than centered composite designs

Energy measurements during welding were acquired during the deposition of the sixth layer for all conditions and alloys. The choice to use the sixth band is to properly represent the welding energy between a previously welded strip while minimizing the possible effects of the welding plate. Additionally, consideration of energy in a specific layer eliminates the need to account for energy loss as a function of height for single band specimens. Unfortunately, alloy AA5056 quickly proved to be impossible to weld as it will be discussed below. Table 7 summarizes the results based on the levels discussed previously (Table 5).

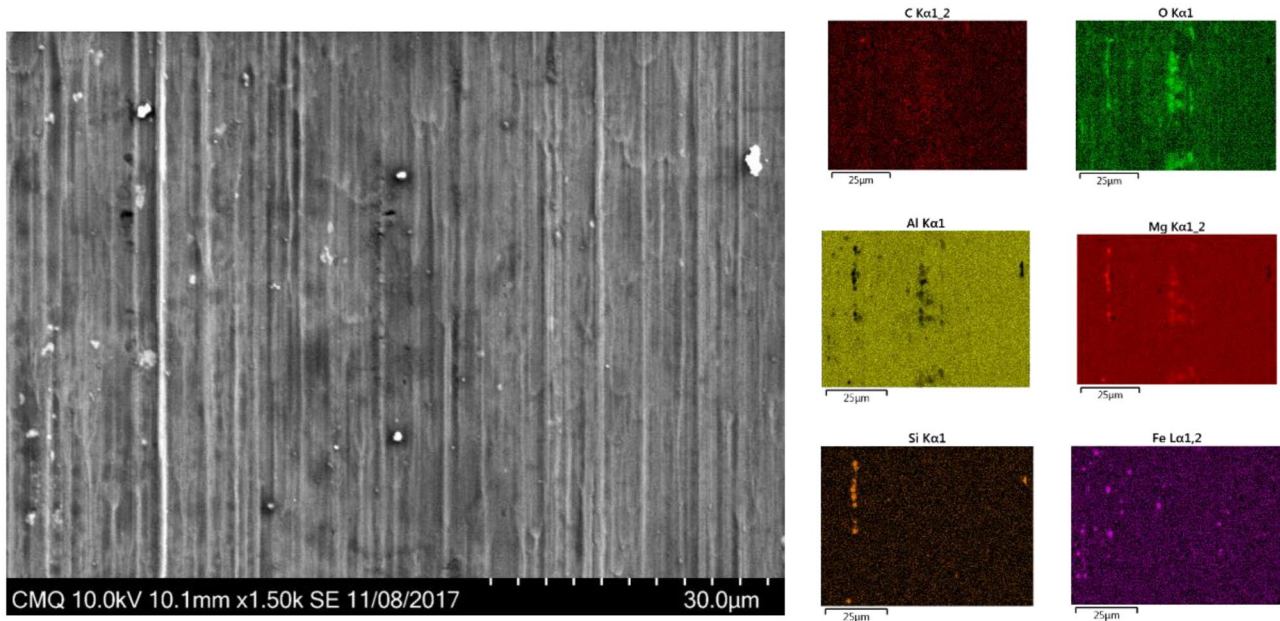


**Fig. 10** SEM micrograph of the surface of a AA5056-H38 alloy strip (TL-L plan) in the “as-received” condition with corresponding X-ray maps

Upon statistical analysis not presented here, it turns out that only four parameters are significant at a 95% confidence level. For the cases of alloys AA5005 and AA5052, it is exactly the same parameters:  $\beta_0$  the ordinate at the origin,  $\beta_2$  the feed rate,  $\beta_3$  the amplitude of oscillation, and  $\beta_{22}$  the value of the feed rate squared. The general equation for the energy estimate (Eq. 2) is first displayed followed by the normalized regressions found for the respective alloys (Eqs. 3 and 4). According to the hypothesis tests, the two models consist only of significant effects and are adequate.

$$E = \beta_0 + \beta_2 x_2 + \beta_3 x_3 + \beta_{22} x_2^2 \quad (2)$$

$$E_{AA5005-H38} = 62,8 - 14,5x_2 + 8,69x_3 + 3,61x_2^2 \quad (3)$$

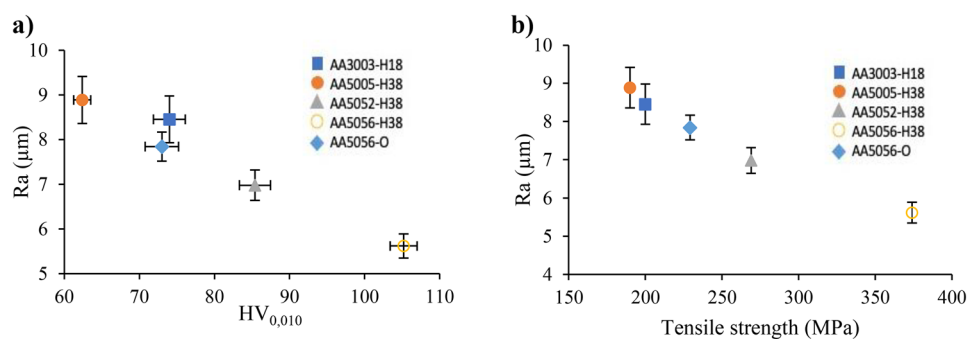
$$E_{AA5052-H38} = 47,3 - 9,82x_2 + 8,68x_3 + 4,19x_2^2 \quad (4)$$

The coefficients of determination ( $R^2$ ) of Eqs. 3 and 4 are 0.99 and 0.95, respectively. Similarly, the adjusted coefficients

of determination are 0.98 and 0.93. Figure 16 shows the surface response for each regression to facilitate visualization of the quadratic effect, where the blue surface represents alloy AA5005-H38, and the red one is for alloy AA5052-H38. The lateral shift of the surfaces as a function of amplitude arises from the difference between the levels used to characterize the oscillation amplitude (Table 5). These surfaces are very similar both visually and mathematically but have no intersection point. At the same feed rate, but 5% less amplitude, alloy AA5005-H38 requires more energy. This trend is also identical over the entire parameter range. Within the common parametric interval of the two surfaces, either for an oscillation amplitude between 32.8 and 35  $\mu\text{m}$  as well as for a feed rate between 64 and 106 mm/s, the energy to deposit alloy AA5052-H38 is on average 24 J/cm<sup>2</sup> lower than that for alloy AA5005-H38. For both alloys, the energy registered by the welding unit is higher when the feed rate is reduced or when the amplitude of oscillation is increased.

Undoubtedly the welding parameters have a significant importance on the amount of energy transferred. The

**Fig. 11** (a) Arithmetic roughness of the strip surface after welding as a function of its initial hardness; (b) arithmetic roughness of the strip after passing the sonotrode as a function of its tensile strength ( $F=5$  kN,  $f=85$  mm/s,  $a=35$   $\mu\text{m}$ )



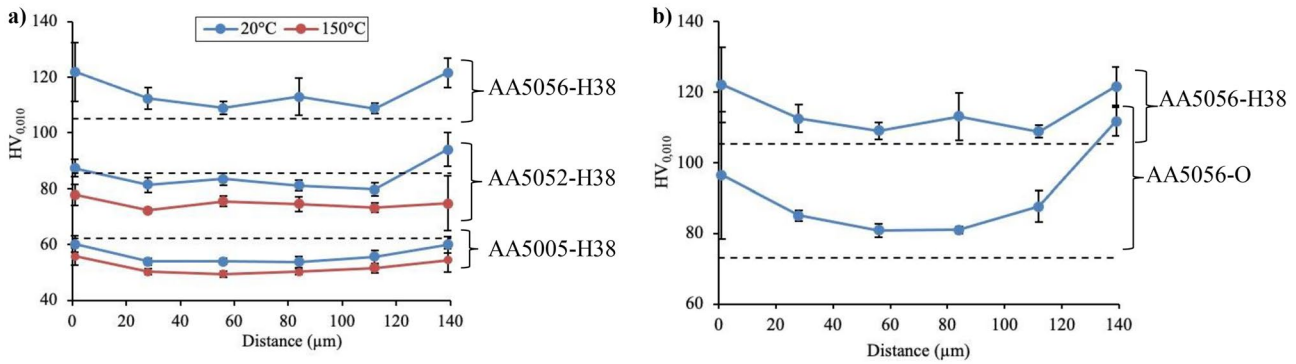


**Fig. 12** Microhardness profiles across the thickness of a welded strip in the YZ plane: **(a)** comparison between the three Al–Mg alloys studied at two deposition temperatures; **(b)** comparison between

AA5056 specimens in the strain-hardened and annealed conditions (5 kN, 85 mm/s, and amplitude of 35 μm)

regressions obtained explain the inability of the apparatus to weld the AA5005-H38 alloy at room temperature for very high amplitudes of oscillations combined with a slower deposition rate. These conditions force the welding unit to trip regularly due to energy requirements that are too important. Based on the results presented in Fig. 16, it was decided to consider the cases of “minimum energy” and “maximum energy” to determine the range of tensile properties that can be obtained within the span of parameters studied.

### 3.5 Longitudinal tensile properties of single band specimens as a function of deposition parameters

As discussed previously, the choice of parameters influences the energy transmitted depending on the strips used. This energy change in turn causes certain differences, among other things on roughness and hardness, but also on the tensile properties. The limiting energy levels from the range of parameters (Table 5) were tested under two temperatures, i.e., 20 °C and at 150 °C, on single band specimens. The stress–strain curves are shown in Fig. 17. Numerical values for yield strength, ultimate tensile strength, and elongation are reported in Table 8. The preheated samples of each alloy were submitted to exactly the same preheating temperature as well as the same exposure time.

The properties of alloy AA5005-H38 are strongly influenced by the welding parameters and the preheating temperature used. Alloy AA5052-H38 exhibits identical tensile strengths for the minimum and maximum energy parameters, where a similar trend is observed for its elongation. It seems to be more dependent on preheating than on welding parameters. In addition, this alloy shows streaks on its tensile curve, a common phenomenon in Al–Mg alloys [23] but amplified here by the presence of several interfaces that gradually break over the course of the tensile test.

### 3.6 Tensile properties of block specimens

The tensile properties obtained for the longitudinal and long transverse directions when fabricating blocks under the same standard parameters are shown in Fig. 18 and Table 9. The results for the deposition direction are also included in this table. The notion of minimum and maximum energy as a function of the number of deposited strips does not apply in the case of block specimens as highlighted in Fig. 15.

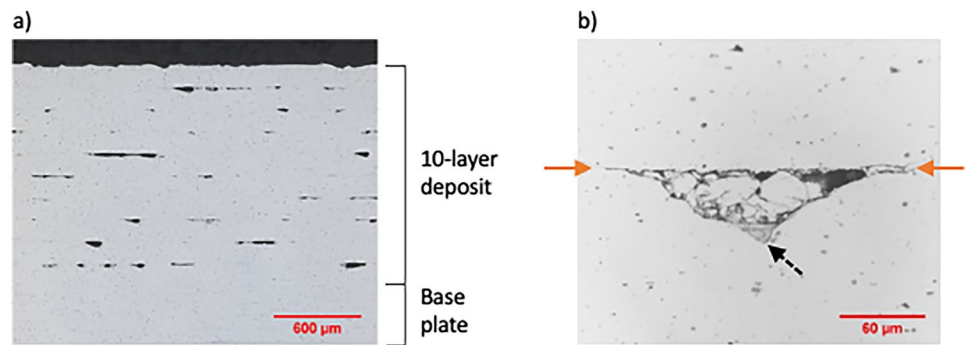
For the three alloys tested, a notable decrease in elongation is visible in the short transverse direction. A significant reduction in tensile properties in the direction of construction of the blocks is also visible compared to other directions. For identical production parameters, alloy AA3003-H18 exhibits mechanical properties superior to alloy AA5005-H38, even though the former has lower tensile strengths and is less sensitive to strain hardening.

**Table 6** Maximum height achieved by UWAM as a function alloy chemistry and sample type

Sample series	Deposit	AA3003-H18	AA5005-H38	AA5052-H38	AA5056-H38	AA5056-O
Single bands	Height deposited (mm)	19	19	7	1.5*	1.5*
	Potential of depositing more layers?	Yes	Hardly	No	No	No
Blocks	Height deposited (mm)	7	7	7	-	-
	Potential of depositing more layers?	Yes	Yes	No	-	-

\*Poor adhesion

**Fig. 13** a) Low-magnification micrograph of the YZ plane for a specimen of AA5056-H38 alloy under standard deposition parameters ( $F=5\,000\text{ N}$ ,  $f=85\text{ mm/s}$ ,  $a=35\text{ mm}$ ), b) micrograph acquired at higher magnification showing the presence of debris and an oxide inclusion (arrowed) at the interface between two neighbouring strips



It also yields properties similar to those of alloy AA5052-H38 in the long transverse direction. On the other hand, alloys AA3003-H18 and AA5005-H38 provide equivalent tensile properties in the longitudinal and long transverse directions.

The increased magnesium concentration also produces more visible defects at the interfaces when the strips are layered in the Y-direction, which is necessary for the production of the block specimens. The joints show much less deformation in the case of the AA5052-H38 alloy, are more angular, and above all are much more discernible following the observation of the fracture surfaces (Fig. 19). The micrographs in Fig. 19a, b show the general aspect of the fracture surfaces, while those in Fig. 19c, d show a joint between neighboring strips at higher magnification.

### 3.7 Effect of deposition parameters on tensile properties in the short transverse direction

The material deposition direction (Z) corresponds to the short transverse direction of the strips. This direction is particularly problematic to characterize in traction with standard tests for two main reasons: (1) the time required to produce samples and (2) the weldability for the overall thickness required.

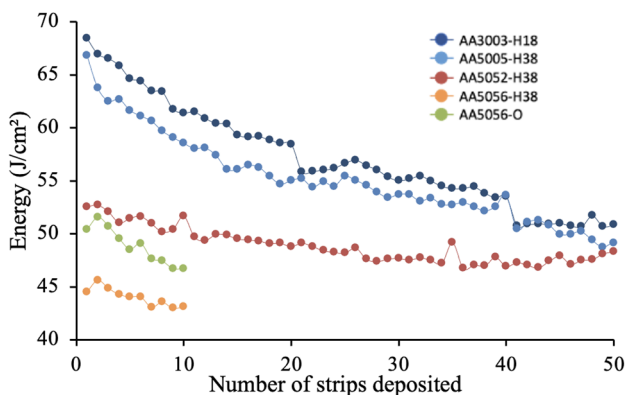


**Fig. 14** Energy supplied as a function of specimen thickness for single band specimens built at room temperature, using standard UWAM parameters ( $F=5000\text{ N}$ ,  $f=85\text{ mm/s}$ ,  $a=35\text{ }\mu\text{m}$ )

The minimum length required by ASTM E8/E8M for flat tensile test specimens is 100 mm. The use of a baseplate of at most half this thickness does not solve the problem, since it is impossible, with some of the alloys studied here, to deposit 50 mm of material. Such deposit thickness could possibly be attainable by using a wider structure, thus limiting lateral vibrations of the entire specimen. The latter option was not considered in this study.

The tensile strength, for nonstandard specimens, was characterized according to a full factorial  $2^3$  design of experiments (ref. Table 10). The parameters under study are the normal force, the feed rate and the oscillation amplitude, still according to the levels presented in Table 5. The use of such a design of experiments allowed the identification of a maximum of seven effects excluding the intercept. It is therefore possible to obtain the individual effects for parameters 1, 2, and 3 as well as the combined effects 12, 13, 23, and 123. In total, 37 tests were performed for alloy AA5005-H38, while 43 tests were performed for alloy AA5052-H38.

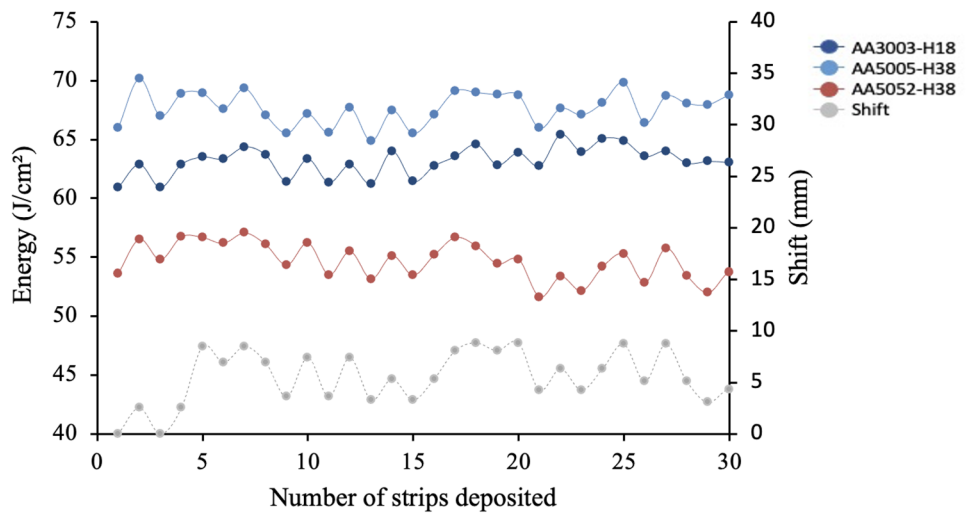
Following the complete statistical evaluation of the results for the two alloys, only the individual effects related to feed rate ( $x_2$ ) and amplitude ( $x_3$ ) are significant at 5%. The regressions determined from the normalized design are given by Eqs. 5 and 6, and the response surfaces are shown in Fig. 20.

$$UTS_{5005-H38} = 36,7 - 10,4x_2 + 11,5x_3(\text{MPa}) \quad (5)$$

$$UTS_{5052-H38} = 64,0 - 6,93x_2 + 11,7x_3(\text{MPa}) \quad (6)$$

Increasing the strength of the welds in pure tension is therefore possible, for both alloys, by reducing the feed rate as well as increasing the amplitude of oscillation. The mathematical relationships obtained, although statistically adequate at the 5% threshold, do not accurately reflect the situation encountered. The AA5005-H38 alloy regression has a coefficient of determination ( $R^2$ ) of 0.56 and a much lower adjusted coefficient of determination of approximately 0.38. Alloy AA5052-H38, on the other hand, shows a better correlation with a coefficient of determination of 0.66 and adjusted to 0.55. Notable standard deviations, especially in

**Fig. 15** Energy supplied as a function of specimen thickness for block specimens built at room temperature using standard UWAM parameters ( $F=5000\text{ N}$ ,  $f=85\text{ mm/s}$ ,  $a=35\text{ }\mu\text{m}$ )



the case of AA5005-H38, are present and sometimes as large as 48% of the value of the response obtained. It is therefore very difficult to represent the situation adequately with such results. This significant variation is mainly due to the use of a very small area analyzed during tensile tests ( $<1\text{ mm}^2$ ), heavily affected by a slight lack of cohesion between the strips. Based on the results of the regressions performed, alloy AA5052-H38 offers tensile strengths on average 36 MPa higher than alloy AA5005-H38. The properties of alloy AA5052-H38 are therefore slightly more than twice those of alloy AA5005-H38 when welded at room temperature using the same deposition conditions.

Despite the small size of the specimens used, it is possible to see on several layers the manifestation of plastic deformation induced by the tensile test. Figure 21 shows the microstructure of a miniature tensile specimen of alloy

AA5005-H38 manufactured using parameters  $(-1: -1:1)$ . This is the combination of parameters that resulted in the highest average stress for this type of test. Without being completely ruptured, this deformation was sufficient to terminate the test. The interface between the wrought baseplate and the welded strips is indicated by a white arrow.

### 3.8 Optimization of tensile properties for block specimens

The previous sections have exposed the effect of the deposition parameters on the mechanical properties of the joints produced, but also on the tensile properties in the longitudinal and long transverse directions. In order to take advantage of these notions, block specimens were produced with alloy AA5052-H38 under new deposition conditions. The parameters were kept constant throughout the manufacturing sequence since the energy reduction is not observed when producing a block. Here are the parameters chosen and their respective justifications.

- Force: 5000 N

Since the force does not have a significant effect on either the recorded energy or the strength of the joints during the miniature tensile tests, a force sufficient to produce a suitable strain was selected.

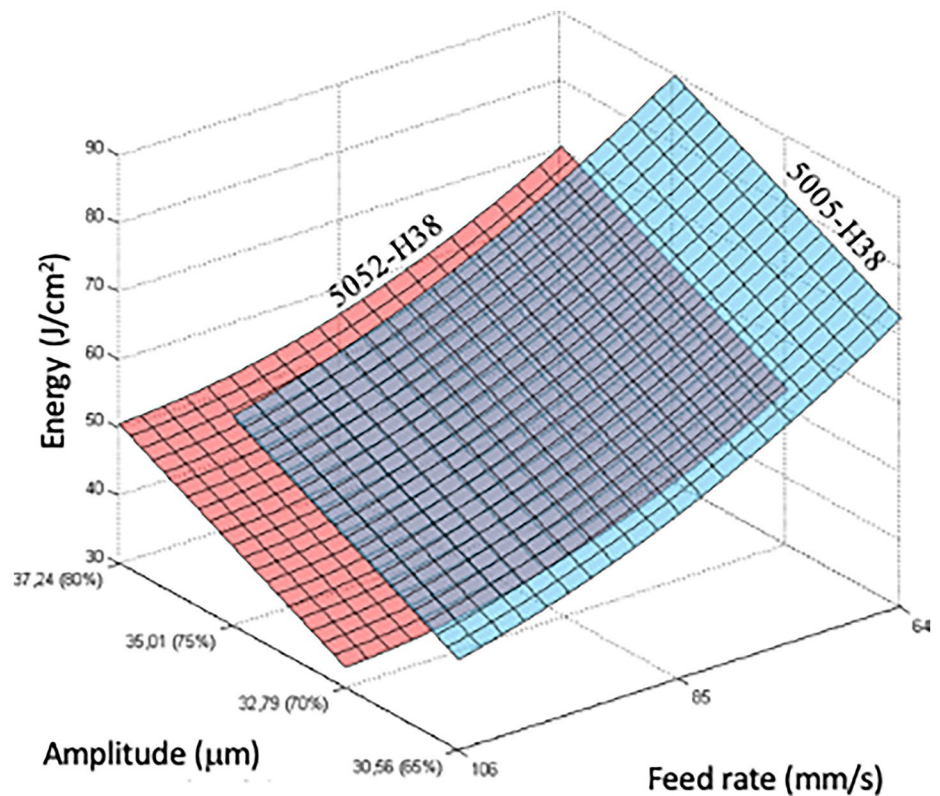
- Feed rate: 47 mm/s

The decrease in feed rate results in increased welding energy and has been shown to benefit the tensile properties of the joints. This value is reduced so as to be much slower than the parameters explored to improve strength along the short transverse direction, but also the long transverse direction based the previous results.

**Table 7** Surface energy to weld single band specimens as a function of deposition parameters for alloys AA5005-H38 and AA5052-H38

Levels			Energy	
Force	Feed rate	Amplitude	AA5005-H38	AA5052-H38
$x_1$	$x_2$	$x_3$	$\text{J/cm}^2$	$\text{J/cm}^2$
-1	-1	0	78.8	58.5
1	-1	0	83.1	60.7
-1	1	0	51.5	42.9
1	1	0	54.0	45.2
-1	0	-1	55.4	42.6
1	0	-1	54.4	38.3
-1	0	1	71.8	62.4
1	0	1	70.8	55.5
0	-1	-1	70.9	57.2
0	1	-1	43.3	33.8
0	-1	1	91.4	73.8
0	1	1	59.6	49.7
0	0	0	62.9	47.3

**Fig. 16** Response surfaces for the regressions approximating the surface energy according to the advance and the amplitude for alloys AA5005-H38 and AA5052-H38



- Amplitude: 35  $\mu\text{m}$

The increase in amplitude also plays a positive role on the tensile properties. On the other hand, the use of a very high amplitude often generates more metal being deposited on the sonotrode and also tends to deflect the strips during welding. A median amplitude was therefore selected in favor of a significant slower feed rate.

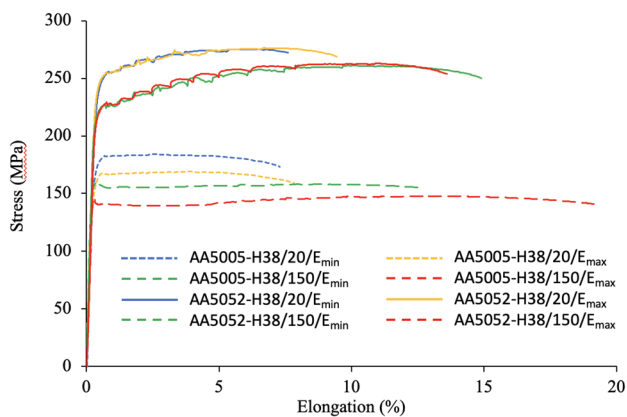


**Fig. 17** Stress–strain curves for single band specimens of alloys AA5005-H38 and AA5052-H38 welded using minimum and maximum energy conditions at 20 and 150 °C. Tensile specimens were sampled along the longitudinal direction

- Temperature: 110°C

The plastic deformation is favored by preheating, but this additional energy induces a reduction of the final properties of the parts in the directions other than that of the deposition. A slightly lower temperature, i.e., 110°C, than that used for the upper level was therefore selected.

The tensile test results for the different orthotropic directions of block specimens are presented in Fig. 22 as well as in Table 11.

The tensile strengths obtained are far greater than those previously determined for alloys AA3003-H18 and AA5005-H38. Compared to alloy AA5052-H38 built at room temperature with standard parameters, a slight decrease in mechanical properties is notable in the longitudinal direction. However, this is largely offset by large gains in the long and short transverse direction. It is also the only sample showing a homogeneous plastic deformation domain along the long transverse direction. The choice of more energetic parameters made it possible to obtain the best properties of all the tests carried out in long transverse and short transverse directions. The significant gain in the long transverse direction is attributable to more significant plastic deformation between the strips, also promoted by the preheating as well as the reduction in feed rate allowing for a longer local exposure time. The use of less preheat as well as a low advance resulted in mean interface hardness values of 85

**Table 8** Results of longitudinal tensile tests for single band samples built following the limit energy parameters. Tensile specimens were sampled along the longitudinal direction

Alloy	Energy	20 °C			150 °C		
		YS (MPa)	UTS (MPa)	EI (%)	YS (MPa)	UTS (MPa)	EI (%)
AA5005-H38	Min	177 ± 3	181 ± 3	10 ± 2	156 ± 4	159 ± 3	19 ± 2
	Max	168 ± 6	174 ± 5	12 ± 1	143 ± 1	149 ± 1	25 ± 1
AA5052-H38	Min	248 ± 2	276 ± 1	8 ± 1	221 ± 2	262 ± 1	18 ± 1
	Max	241 ± 4	275 ± 1	12 ± 1	222 ± 1	262 ± 2	17 ± 1

HV<sub>0.010</sub> and center hardness of 74 HV<sub>0.010</sub>. These numbers are similar to those obtained at the interfaces during deposition at room temperature and similar to those at the heart of the strips during deposition at 150 °C with standard parameters (Fig. 12a).

The use of backscattered electron diffraction (EBSD) on this same sample has revealed the significant grain size refinement at the interfaces. Figure 23a shows a more general area where the full thickness of a strip is visible between two welded interfaces and Fig. 23b a magnification specifically on an interface pointed by red arrows in Fig. 23a. The step used for the mapping in Fig. 23a was 188.6 nm and 82.9 nm in Fig. 23b. Darkened regions are areas of lower indexing. Three more specific regions are identified and represent the strongly deformed zone at the interface due to the passage of the sonotrode and the welding process itself (zone 1), the intact zone in the center of the strip (zone 3), and the intermediate zone (zone 2).

The major part of the observable structure is formed of elongated grains and sub-grains typical of the original microstructure of the strips in their “as-received” condition. In the vicinity of the welded areas, the consequence of significant plastic deformation caused by the passage of the sonotrode is visible along the direction of vibration. This plastic deformation affects only a small volume on either side of the interface to a depth of approximately 20 μm along the direction perpendicular to the initial joint. The deformed

zone is characterized with fine grains that are nearly equiaxed compared to the elongated grains of the strip along the transverse direction, the latter being on average 50-μm long. Visually, the transition between the area affected by the welding formed of fine grains and the intact area is smooth. The large grains seem to be gradually pulled and fragmented toward the weld area to produce new, finer grains. The sub-grains in the center of the strip have an average size of 4.3 μm (zone 3), while the intermediate zone (zone 2) contains sub-grains with an average size of 1.4 μm. The welded interface (zone 1) is formed mainly of grains with an average size of 0.91 μm.

### 4 Discussion

The chemical composition of the strips has an unequivocal influence on the ability of the process to produce quality deposits. In the present study, the effect of magnesium concentration has a visible impact on various aspects, from the initial mechanical properties of the base strips to the inability to obtain a decent weld at high contents.

The use of various experimental designs allowed the determination of the main effects on the strength of the joints produced by UWAM on the alloys AA5005 and AA5052 in the state H38. After statistical analysis, only the welding feed rate and the amplitude of oscillations are significant

**Fig. 18** Stress–strain curves of tensile tests in the longitudinal and short transverse directions for alloys AA3003-H18, AA5005-H38, and AA5052-H38. Specimen fabrication was carried out at room temperature. The graph on the left is a zoomed-in section of the area highlighted with dashed lines on the right

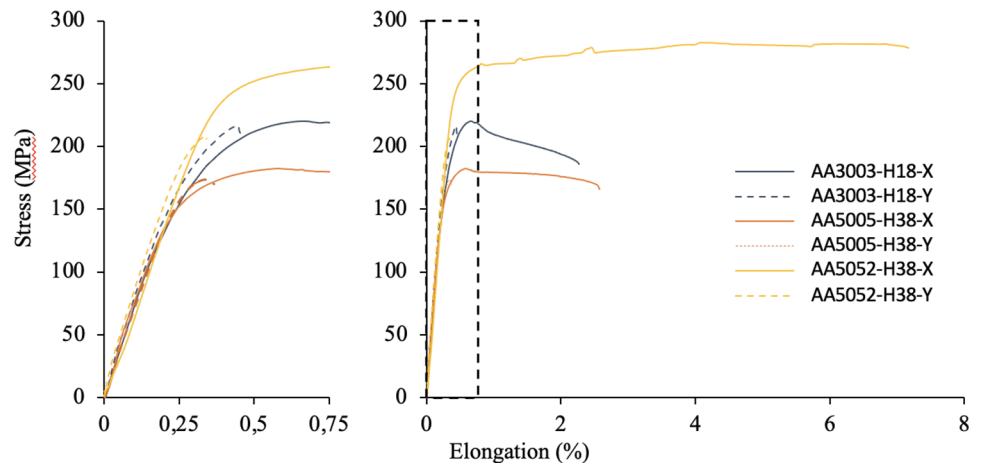


**Table 9** Tensile properties of block specimens according to the longitudinal, long transverse, and short transverse directions for alloys AA3003-H18, AA5005-H38, and AA5052-H38

Alloy	Longitudinal			Long transverse			Short transverse	
	YS (MPa)	UTS (MPa)	EI (%)	YS (MPa)	UTS (MPa)	AI (%)	UTS (MPa)	EI (%)
3003-H18	209 ± 3	221 ± 2	6 ± 1	-	211 ± 9	3 ± 1	64 ± 15	< 1
5005-H38	181 ± 5	187 ± 6	8 ± 2	-	180 ± 7	3 ± 1	57 ± 13	< 1
5052-H38	252 ± 5	281 ± 2	11 ± 2	-	208 ± 4	3 ± 2	69 ± 3	-

during the characterization of tensile properties of joints by miniature tensile tests.

The two tests converge toward the same result whereby the strength of the joints can be increased by increasing the welding energy through the production parameters. This increase can come from a preheating, or simply from the reduction in the forward speed, coupled or not with an increase in the amplitude of oscillation. When using the parametric range presented in Table 5, the best specimens produced for alloys AA5005-H38 and AA5052-H38 only have average tensile strengths of 70 and 86 MPa, respectively. These are 39 and 32% of the initial mechanical properties of the strips. They were both obtained for maximum energy levels, i.e., normal force and maximum amplitude, with minimum feed rate. The use of preheating and a considerably reduced feed rate for the production of sample AA5052-H38 built at 110 °C resulted in an average

tensile strength of 120 MPa or 45% of the value of the base material.

Although beneficial for the tensile properties in the short transverse direction, energy increase is not necessarily desirable for the tensile properties in other directions. During ultrasonic welding of alloy AA5005-H38, the tensile properties in the longitudinal direction were shown to be strongly influenced by the deposition parameters under the two temperatures evaluated. This alloy allows a modulation of the mechanical properties as a function of the production parameters, by which an increase in energy gradually decreases the tensile strength in the longitudinal direction but improves ductility. For minimum energy parameters at 20 °C, the tensile strength in the longitudinal direction is identical to that of the initial strips, but the elongation is 10 times greater. If the preheating temperature is raised to 150 °C and the UWAM parameters are those offering the

**Fig. 19** Typical fracture surfaces along the YZ plane (longitudinal tensile specimens) for sample AA5005-H38 (a and c) and AA5052-H38 (b and d) built using standard welding parameters at room temperature

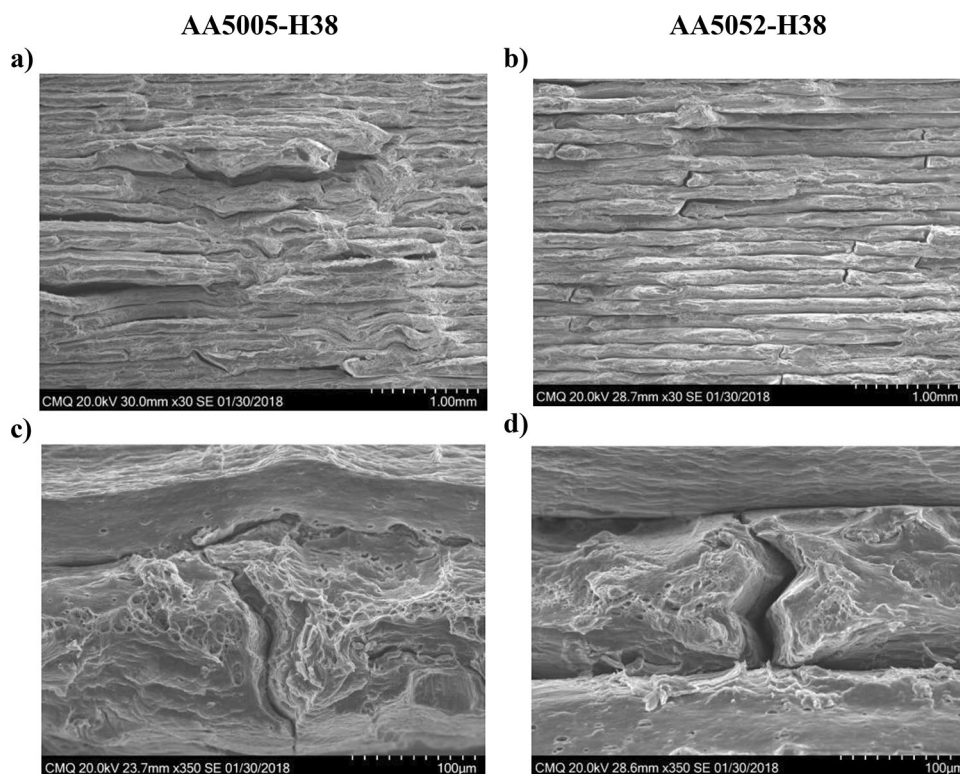


**Table 10** Results of the full standardized experimental design  $2^3$  of the tensile strength of miniature tensile specimens of alloys AA5005-H38 and AA5052-H38 built at room temperature

Force $x_1$	Feed rate $x_2$	Amplitude $x_3$	AA5005-H38 AverageUTS (MPa)	AA5052-H38 AverageUTS (MPa)
1	1	1	$51 \pm 14$	$69 \pm 7$
-1	1	1	$27 \pm 8$	$74 \pm 13$
1	-1	1	$54 \pm 26$	$73 \pm 19$
-1	-1	1	$70 \pm 8$	$86 \pm 6$
1	1	-1	$28 \pm 7$	$42 \pm 6$
-1	1	-1	$16 \pm 8$	$43 \pm 13$
1	-1	-1	$37 \pm 17$	$64 \pm 12$
-1	-1	-1	$35 \pm 7$	$59 \pm 5$
0	0	0	$26 \pm 15$	$69 \pm 3$

maximum energy conditions, the tensile strength decreases slightly to 83% for an elongation equivalent to 25 times that of the metallic strip in its initial H38 condition.

Not being influenced by production parameters like AA5005-H38, alloy AA5052-H38 which has a Mg concentration in solid solution three times higher, is only affected by the preheating temperature. When welded at room temperature, the longitudinal tensile strength is equivalent and sometimes even greater than the properties of the strips with an elongation also 4 times greater. When the preheating temperature is raised to 150 °C,

**Fig. 20** Response surfaces calculated for the regressions approximating tensile strength along the short transverse directions for alloys AA5005-H38 (blue) and AA5052-H38 (red)

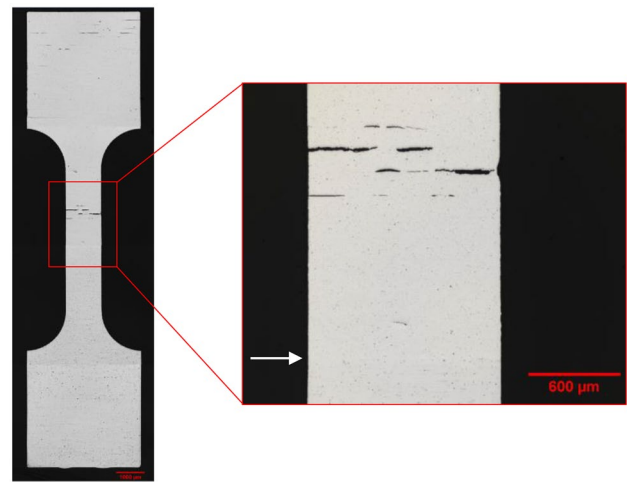
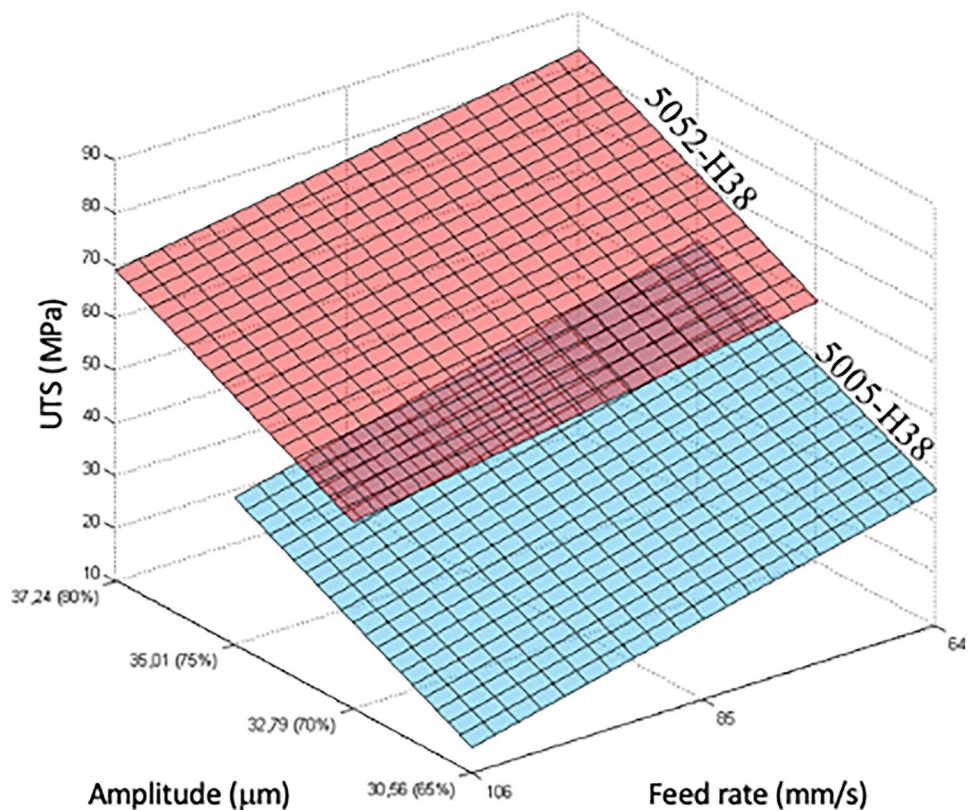
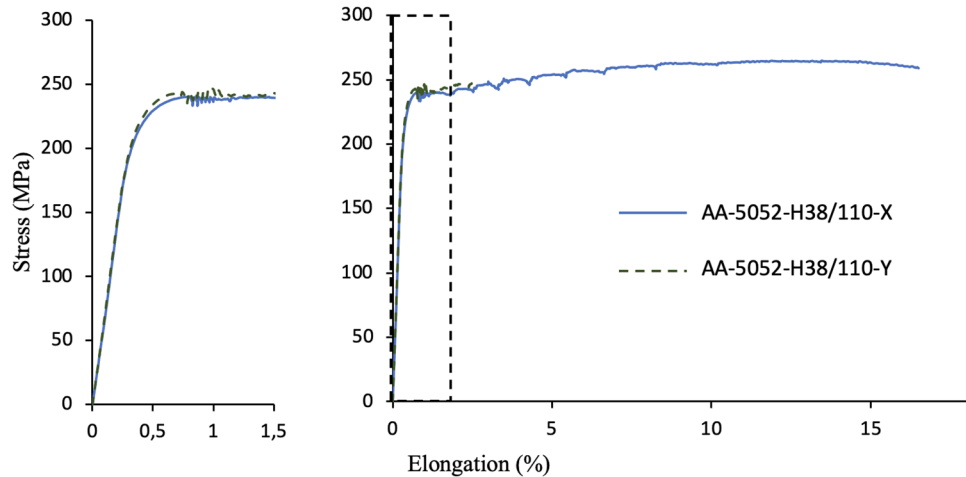


**Fig. 21** Micrograph of a miniature tensile specimen made of alloy AA5005-H38 taken along the short transverse direction

tensile strength slightly decreases to 97% of the initial properties with an elongation 9 times higher. The use of a preheat offers significant benefits.

When producing blocks, the alloys tested exhibit a more brittle behavior in the long transverse direction compared to the longitudinal direction. This characteristic is all the more visible with the increase in Mg concentration for standard deposition parameters at room temperature. The

**Fig. 22** Longitudinal and transverse tensile curves for sample AA5052-H38 built at 110°C. The graph on the left is a zoomed-in section of the area highlighted with dashed lines on the right



properties obtained are highly anisotropic and are strongly influenced by both the manufacturing method used, continuously depositing the strips along the longitudinal axis, and the initial anisotropy of the strips. For identical production parameters, alloy AA5005-H38 provides tensile strengths in the longitudinal and long transverse directions equivalent to those of the base material (strips in the as-received condition). On the other hand, elongation is almost 3 times higher in the longitudinal direction than in the long transverse direction. For alloy AA5052-H38, the longitudinal properties are also similar to strips with equal or greater tensile strength as well as with slightly more than 5 times the elongation. Strength decreases rapidly in the long transverse direction reaching only 77% of the initial properties. This condition is mainly caused by a lack of adhesion at the locations where strips overlap. Welds of lower quality are visible during sample fabrication, where this type of defect is shown in Fig. 24. The last joint was welded according to layer  $n$ , and the offset of the previous layers is still visible even after the overlapping of several bands. These welds produce a fracture profiles in which the offset pattern is discernible explaining the significant decrease in tensile strength (Fig. 25).

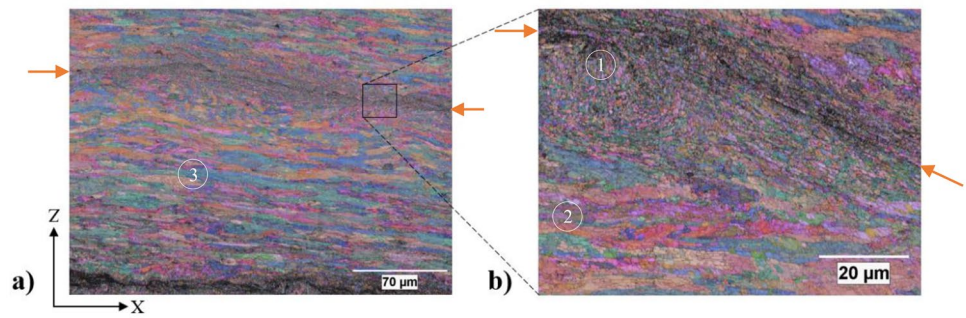
This problem was greatly reduced during the production of the AA5052-H38 blocks built by preheating the specimen to 110 °C and significantly reducing the feed rate. Through these parameters, it is the only welded block showing homogeneous plastic strain of 7% before fracture in the long transverse direction.

With 4.9%-wt. of magnesium, alloy AA5056-H38 is the only alloy in this study that could not be deposited to build specimens of acceptable thickness. Compared to the other alloys characterized, it has a higher hardness under the state H38. Following the passage of the sonotrode, this alloy shows very little change in surface finish (roughness). Partial annealing was used with the aim of reducing the mechanical properties of the strip to the same level as those of the other alloys studied. On the other hand, even with tensile properties and hardness values falling between those of alloys AA5005-H38 and AA5052-H38, it was not possible to create suitable welding between overlaid strips. The reason preventing the creation of strong bonds for this high magnesium alloy is therefore not related to the initial mechanical properties. This aspect is also confirmed by the attempts made to deposit the material at 150 °C where the properties of the typical AA5056-H38 alloy were significantly lower than those of alloy AA5052-H38 produced at room temperature (ref. Table 4) [17]. Thus, alloy AA5056-H38 proved to be impossible to weld as much to itself as to any other alloy presented in this study, including the base-plate. Additionally, according to calculations of the surface stress from the Hertz contact presented in Table 12 [24], the maximum surface stress generated by the sonotrode using the parameters used is 282 MPa for alloy AA5056-H38, which is much greater than the yield strength of alloys AA5056-O and AA5056-H38 at 150 °C, which are 117 MPa and 214 MPa, respectively [17]. The capability of plastically deforming a metallic strip by UWAM is

**Table 11** Tensile properties of sample AA5052-H38 built at 110°C

Longitudinal			Long transverse			Short transverse	
YS	UTS	EI	YS	UTS	EI	UTS	EI
(MPa)	(MPa)	(%)	(MPa)	(MPa)	(%)	(MPa)	(%)
237±6	268±3	21±2	237±2	247±2	7±0.2	120±11	<1

**Fig. 23** EBSD map in band contrast and Euler angles of specimen B52-110 according to the YZ plane in (a) general view and (b) magnification on an interface



therefore not a criterion for determining the weldability of these alloys.

Ultrasound-assisted welding of alloys AA3003-H18, AA5005-H38, and AA5052-H38 results in components that are dense and contain few defects. On the other hand, when using alloy AA5056 in its H38 or annealed states, the number of defects at the interfaces between overlapping strips quickly becomes significant as seen in Fig. 13. The defects, corresponding to the dark regions in Fig. 13a, are concavities left by the passage of the sonotrode, still vacant following the deposition of the subsequent strip due to lack of plastic flow. Several lumps of matter remain trapped within these concavities, a phenomenon absent or rarely encountered for the other alloys studied. A typical cluster trapped between two overlapping strips is arrowed in Fig. 13b, where a residual oxide layer is pointed by a dashed arrow. The numerous visible defects combined with the presence of debris suggest that the strips slide over each other rather than being deformed during ultrasound-assisted welding.

This lack of deformation visible in the YZ plane is also transposed to the XY plane. During the passage of the sonotrode, the strips of grade AA5056-H38 are only slightly deformed, thereby leaving them with significantly lower arithmetic roughness than the other 3 alloys studied (ref. Fig. 11). Energy-dispersive X-ray

spectrometry (EDS) analysis was performed on a welded joint following the peeling of strips immediately before its insertion into the chamber of the scanning electron microscope (SEM). Figure 26 shows a large proportion of intact areas, even after the passage of the sonotrode as well as after the strip has been welded on the same surface. The furrows left by rolling in the longitudinal direction are still visible. Analysis at low acceleration voltage reveals a concentration of Mg in the welded zone (zone 1) identical to that of the base strip (Table 13), while a significant increase in oxygen and magnesium at the intact interface (zone 2) is present. On the other hand, it is impossible to state the exact composition of the oxide, possibly MgO or MgAl<sub>2</sub>O<sub>4</sub> since the interaction volume of the backscattered electrons includes part of the matrix due to its thinness.

The increase in magnesium in the base material (strips) promotes the formation of Mg-rich oxides on its surface. During the welding operation, the diffusion of magnesium is possibly stimulated by vibrations and by the heat generated at the interface between overlapping strips. As the strips are very thin, these factors can

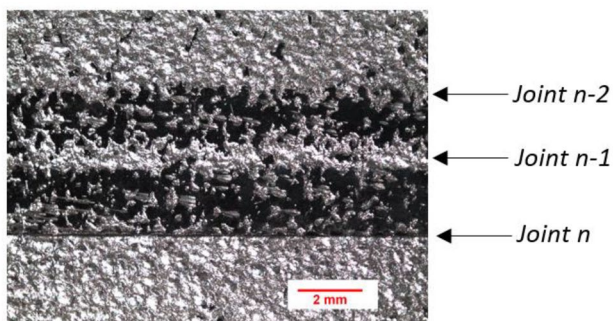


**Fig. 24** Defects visible when shifting layers for the production of sample AA5052-H38 built at room temperature

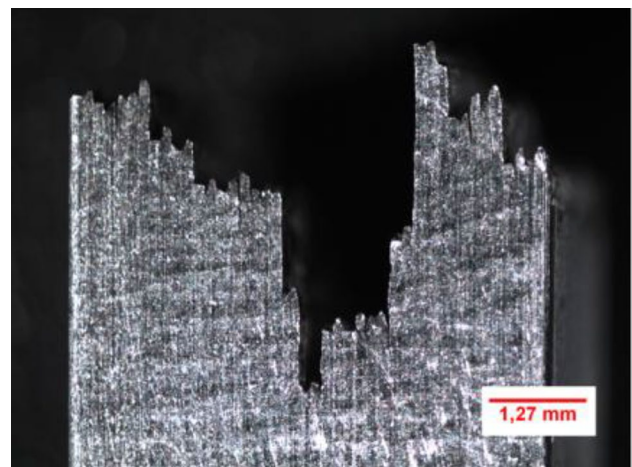


**Fig. 25** Failure profile of a tension in the long transverse direction of sample AA5052-H38 deposited at room temperature

**Table 12** Surface stress developed in the area of contact during UWAM as a function of the normal force applied for the Al–Mg alloys studied

Normal force (N)	AA5005-H38 (MPa)	AA5052-H38 (MPa)	AA5056-H38 (MPa)
4000	227	228	230
5000	253	255	257
6000	278	279	282

be important when depositing multiple layers. In addition to the oxide already present in the base material, UWAM most likely contributes to the formation of additional MgO and/or MgAl<sub>2</sub>O<sub>4</sub> limiting adhesion between the strips. Combined with a rapid rate of welding, the exposure time for the formation of welds is too short to sufficiently disperse the oxide on the surface leaving room for a significant volume fraction of defects. Additionally, the high strain hardening behavior of this alloy reduces plastic deformation achievable at the interfaces, which in return hinders filling of the surface cavities. The increasing presence of magnesium oxide on the surface of the strips is reflected in the results of the tensile tests performed on specimens of alloys AA5005-H38 and AA5052-H38. Indeed, tensile curves clearly show the presence of serration in the case of the latter alloy compared to alloy AA-5005-H38. These serrations are mainly the result of the progressive breakage of the discontinuous welded areas, identical in morphology to those shown in the micrograph of Fig. 26 for the case of alloy AA5056-H38. The absence of serrations for the lower magnesium alloys reflects the achievement of better, more sound microstructures.

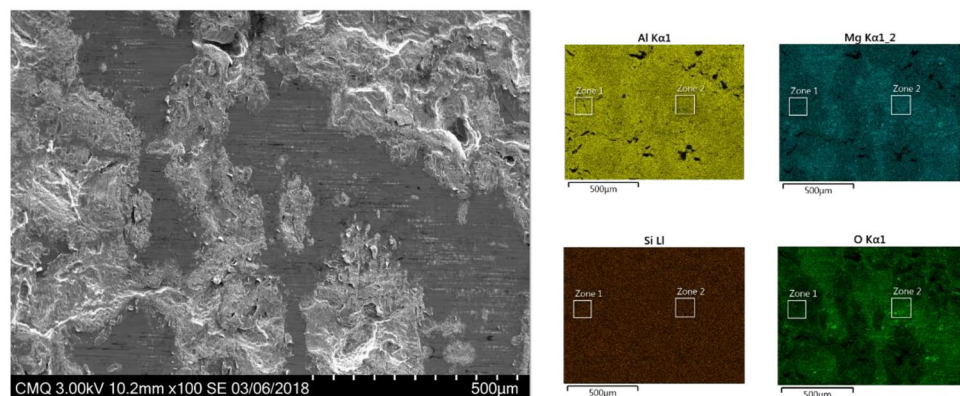
Finally, an additional mechanism that can intervene on the decrease in weldability is recrystallization, more specifically dynamic recrystallization by the progressive rotation of crystal structure, commonly found in Al–Mg alloys for severe deformations [22]. This mechanism

**Table 13** EDS X-ray analysis (%-wt.) of welded and non-welded areas

Area characterized		Al	Mg	O
Zone 1	Zone of deformation	91.0	4.9	4.1
Zone 2	Zone intact	82.7	8.4	9.0

allows the formation of a structure ranging from partially to completely recrystallized grains resulting from the rotation of the sub-grains present in the material. Following significant deformations, this mechanism transforms the sub-grains into new fine-sized grains. In cases where recrystallization is only partial, it occurs first around the grain contour, leaving its center intact or with only a few residual sub-grains. This trend was also observed in the study from Schick [4]. In addition, the new grains are anchored by the second-phase particles present in addition to the fragmented and dispersed oxide.

In the present study, the EBSD mapping for a specimen made of AA5052-H38 built at 110 °C (Fig. 23) shows the presence of numerous sub-grains in the base material transforming into distinct grains in the vicinity of the weld. Since the hardness values near the welds are similar to those of the base material, and since the grain size near the weld is significantly smaller than in the bulk of the strips, it is clear that recrystallization occurred over a short distance on both sides of the weld. Comparing the results of Fig. 23 and the hardness profiles of Fig. 12, it is seen that the high Mg concentration in alloy AA5056-H38 prevents recrystallization from taking place since the recrystallization temperature increases with the content of alloying elements. The use of a preheater in conjunction with parameters that induce high-energy transfer to the strip were not sufficient to reach the activation energy required for this recrystallization to take place. Recrystallization also explains why significant elongation values were obtained following welding compared to those of the initial strips.

**Fig. 26** SEM micrograph (secondary electron imaging) and corresponding EDS X-ray maps of the surface of a strip alloy AA5056-H38 deposited at room temperature and peeled off prior to characterization

## 5 Conclusion

The work summarized above dealt with the characterization of the ultrasonic additive manufacturing process for the production of aluminum components made of alloys from the AA5000 series. Alloys AA5005 and AA5052 in the H38 made it possible to obtain solid joints and therefore adequate tensile properties. On the other hand, alloy AA5056 could not be welded adequately within the framework of this study. When welded under the same parameters, the increase in the magnesium content in the H38 strips resulted in a decrease in the surface roughness left by the sonotrode and rapidly increased the hardness values measured near interfaces between superimposed layers.

Design of experiments was used to determine the effect of the principal UWAM parameters on the welding energy supplied to the metallic strips and their effect on tensile properties of the built specimens.

- The significant parameters for the estimation of energy for alloy AA5005-H38 and alloy AA5052-H38 are the feed rate and the amplitude of oscillation, the normal force having no significant impact. The energy increase is possible by reducing the feed rate and/or increasing the amplitude of oscillation.
- The same conclusions apply to the measurement of tensile properties by the use of miniature tensile test specimens for these two alloys.

As a result of the deposition direction and the use of highly strain-hardened metallic strips, the parts produced are highly anisotropic. Comparison of the tensile properties of the block specimens vs. the layered strips specimens yields the following conclusions:

- 5% increase of tensile properties in the longitudinal (X) direction compared to the as-received strips with elongations up to 25%
- Identical tensile properties than the as-received strips the in the long transverse direction (Y) with elongations of 7%
- Up to 55% lower tensile properties in the short transverse direction (Z) compared to the properties of the as-received strips

Energy loss is visible when building single bands, a phenomenon that is not observed when welding larger structures. This loss follows a quadratic trend as a function of the number of layers deposited by UWAM.

Finally, the UWAM process exhibits inability to properly build specimens of AA5056-H38 alloy under the parameters studied. This is mainly explained by the

presence of magnesium oxide on the surface of the strips and the inability of the process to adequately break up and disperse the oxides on the surface. Plastic deformation is also hampered by the higher Mg concentration which has the effect of preventing recrystallization from taking place and increasing strain hardening. All these mechanisms participate to limit plastic strain at the interfaces and reduce the surface area of welds between overlapping strips.

**Funding** The authors would like to thank the Quebec Metallurgy Center and the Mitacs Accelerate Program (grant # 1617–15837 RM) as well as the REGAL-Aluminum Research Center for their financial support. Mitacs, 1617–15837 RM, Carl Blais, Quebec Metallurgy Center, 1617–15837 RM, Carl Blais, REGAL-Research Center, 1617–15837 RM, Carl Blais

**Availability of data and materials** The raw/processed data required to reproduce these findings cannot be shared at this time as the data also forms part of an ongoing study.

## Declarations

**Ethics approval** Not applicable.

**Consent to participate** Not applicable.

**Consent for publication** Not applicable.

**Competing interests** The authors declare no competing interests.

## References

1. Wolcott P (2015) Ultrasonic additive manufacturing: Weld optimization for aluminum 6061, development of scarf joints for aluminum sheet metal, and joining of high strength metals
2. Fabrisonic (2016) How it works. Online Available at: <http://fabrisonic.com/uam-overview/>. Accessed on 16th Dec 2020
3. Kong CY, Soar RC, Dickens PM (2004) Optimum process parameters for ultrasonic consolidation of 3003 aluminium. *J mater process technol* 146:181–187
4. Schick DE (2009) Characterization of aluminum 3003 ultrasonic additive manufacturing. Ohio State University
5. Schick DE, Hahnen RM, Dehoff R, Collins P, Babu SS, Dapino MJ, Lippold JC (2010) Microstructural characterization of bonding interfaces in aluminum 3003 blocks fabricated by ultrasonic additive manufacturing. *Welding Journal* 89(1S):105–115
6. Siddiq A, Ghassemieh E (2011) Fibre embedding in aluminium alloy 3003 using ultrasonic consolidation process—thermo-mechanical analyses. *Int J Adv Manuf Technol* 54:997–1009
7. Zhang C, Li L (2008) A Friction-Based finite element analysis of ultrasonic consolidation. *Welding Research* 87(1S):187–194
8. Janaki Ram G, Yan Y, George J, Robinson C, Stucker B (2006) Improving linear weld density in ultrasonically consolidated parts. Utah State University, Utah
9. Friel R, Johnson K, Dickens P, Harris R (2010) The effect of interface topography for ultrasonic consolidation of aluminum. *Mater Sci Eng* 527(1A):4474–4483

10. Li D, Soar R (2008) Plastic flow and work hardening of Al alloy matrices during ultrasonic consolidation fibre embedding process. *Mater Sci Eng* 498(1A):421–429
11. Mariani E, Ghassemieh E (2010) Microstructure evolution of 6061-O Al alloy during ultrasonic consolidation: An insight from electron backscatter diffraction. *Acta Materialia* 58:2492–2503
12. Shimizu S, Fujii H, Sato Y, Kokawa H, Sriraman M, Babu S (2014) Mechanism of weld formation during very-high-power ultrasonic additive manufacturing of Al alloy 6061. *Acta Materialia* 74:234–243
13. Zhu Z, Lee K, Wang X (2012) Ultrasonic welding of dissimilar metals, AA6061 and Ti6Al4V. *Int J Adv Manuf Technol* 59:569–574
14. Kong C, Soar R, Dickens P (2005) A model for weld strength in ultrasonically consolidated components. *J Mech Eng Sci* 219(1C):83–91
15. Wolcott P, Hehr A, Pawlowski C, Dapino M (2016) Process improvements and characterization of ultrasonic additive manufactured structures. *J Mater Process Technol* 233:44–52
16. Sridharan N, Gussev M, Seibert R, Parish C, Norfolk M, Terrani K, Babu S (2016) Rationalization of anisotropic mechanical properties of Al-6061 fabricated using ultrasonic additive manufacturing. *Acta Materialia* 117:228–237
17. ASM Handbook (1990) *Metals Handbook vol. 2 - Properties and Selection: Nonferrous Alloys and Special-Purpose Materials*, 10th ed., ASM International, Materials Park, OH, USA
18. ASTM International (2014) *Standard B-209-14 Specification for Aluminium and Aluminium-Alloy Sheet and Plate*, ASTM International, West Conshohocken, PA, USA
19. ASM International (1991) *Metals Handbook vol. 4 - Heat Treating*, 10th ed, ASM International, Materials Park, OH, USA
20. ASTM International (2016) *Standard E8/E8M Test Methods for Tension Testing of Metallic Materials*, ASTM International, West Conshohocken, PA, USA
21. ASM International (2004) *Metals Handbook vol.9 - Metallography and Microstructures*, 10th ed, ASM International, Materials Park, OH, USA
22. Humphreys F, Hatherly M (2004) *Recrystallization and related annealing phenomena*. 2e éd
23. McQueen H, Spigarelli S, Kassner M, Evangelista E (2011) *Hot deformation and processing of aluminum alloys*
24. Budynas RG, Nisbett JK (2006) *Shigley's mechanical engineering design* 8 éd., McGrawHill

**Publisher's Note** Springer Nature remains neutral with regard to jurisdictional claims in published maps and institutional affiliations.